Predissociation and collisional depopulation of the Cs₂(*E*) state

Z. Wu and J. Huennekens

Department of Physics, Princeton University, Princeton, New Jersey 08544

We report here an experimental study of depopulation mechanisms of the Cs$_2$(*E*) state. By combining ratios of atomic to molecular fluorescence with *E* state lifetimes obtained by the phase shift technique, all studied as a function of Cs density, we were able to obtain absolute values for predissociation, radiative, and collisional depopulation rates as well as the total quenching rates for the Cs$_2$(*E*) state. The results are discussed in relation to those of other experiments.

I. INTRODUCTION

Over the past several years there has been much interest in the development of alkali dimer lasers both as a tool for the spectroscopic study of the alkali molecules and as a source of high-power quasitunable light.[1–5] In the latter respect, the heavier alkalis, rubidium and cesium, are of particular interest since the density of molecular energy levels approaches the point where almost continuous tuning may be achieved. Additionally since equivalent transitions lie further to the red in the heavier alkalis, they offer the possibility of high-power quasitunable lasers in the short-wave infrared where at present such sources are scarce and difficult to operate. However, most of the work to data on alkali dimer lasers has concentrated on the lighter alkalis such as sodium.

Recently infrared cross fluorescence (radiative transitions between two excited states) has been observed from Cs$_2$ excited by argon ion laser lines.[6–8] The wavelength range of this cross fluorescence (1.0–2.5 μm), combined with the high spectral density of the emission lines and the convenience of the argon ion laser pump, make these cross fluorescence transitions interesting lasing candidates.

Unfortunately, little is known about the proposed laser levels, although the strongest IR emission between 1.48 and 1.65 μm has recently been identified as the $E\,^1\Sigma_u^+ \rightarrow {}^1\Pi_g$ transition of Cs$_2$.[8] Information on the population and depopulation mechanisms of both of these levels would be useful to assess the potential of this lasing candidate. Consequently we have made a quantitative study of the predissociation, collisional and radiative depopulation rates of the Cs$_2$ (*E*) state which we report here.

Two previous studies of Cs$_2$ (*E*) state decay mechanisms are of great interest in connection with the present experiment. Baumgartner *et al.*[9] made measurements, using the phase-shift technique, of the lifetimes τ of levels pumped by various Ar$^+$ laser lines. Their extrapolation of $1/\tau$ to zero pressure yielded the sum of the radiative and any predissociation decay rates. The fact that different laser wavelengths resulted in different zero pressure extrapolations of $1/\tau$ led them to suggest that the Cs$_2$ "*E*" absorption band may actually consist of more than one electronic transition. The separated atom dissociation limit of these states is probably 7*P* + 6*S*, but no calculations of the relevant potentials has been attempted.

Collins *et al.*[10–12] used a pulsed, two photon technique

to study relative photolysis (photon-induced breakup) rates of the *E*, *D*, and *C* states of the Cs$_2$ molecule to the atomic 5*D* + 6*S* and 6*P* + 6*S* levels as a function of excitation wavelength. Additionally the pulsed, two-photon technique allowed determination of relative photolysis rates to each fine structure level. The experiment we describe here was designed to be complementary to the work of Collins *et al.* in that we obtained absolute predissociation and collisional depopulation rates at three specific wavelengths.

Cs$_2$(*E*) is depopulated in our experiment by radiative decay, predissociation to the 7*S* + 6*S*, 5*D* + 6*S*, and 6*P* + 6*S* atomic levels, and excitation transfer collisions with ground state atoms and molecules. In Sec. II we develop a rate equation model of the Cs$_2$ (*E*) and Cs$_2$ (*A*) state, and atomic 7*S* and 5*D* state populations. These are then used to obtain fluorescence intensity ratios in terms of the various radiative, collisional, and predissociation rates which we wish to determine.

Section III describes the measurements of these fluorescence intensity ratios. Relative measurements of I_{7S}/I_E and I_{5D}/I_E vs Cs density yield the ratio of predissociation to collisional rates, while absolute calibration of I_{7S}/I_E at one density, when combined with the lifetime results of Sec. IV, then yields absolute rates. Measurement of I_A/I_E yields the rate coefficient for

$$\text{Cs}_2(E) + \text{Cs}(6S) \rightarrow \text{Cs}_2(A) + \text{Cs}(6P). \qquad (1)$$
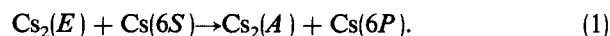
Absolute measurements of the ratio of visible fluorescence to infrared cross fluorescence from the Cs$_2$(*E*) state yield its branching ratios.

In Sec. IV we describe the measurements we made of the Cs$_2$(*E*) state lifetimes using the phase-shift technique. These results, combined with the fluorescence measurements yield the *E* state radiative decay rates and serve as an important consistency check on the predissociation and collisional excitation transfer rates presented. They also provide total quenching rates of the Cs$_2$(*E*) state.

Our results are summarized in Sec. V and in Tables I–III.

II. THEORY

In this section, we consider the various processes occurring in the vapor which are relevant to the population and depopulation of the molecular *E* and *A* states and the atomic 7*S* and 5*D* states (by "*A* state" throughout this paper we

mean the A $^1\Sigma_u^+$, a $^3\Pi_u$, and b $^3\Sigma_g^+$ states of the first excited manifold which we lump together since all three states radiate in the same wavelength region). Other molecular and atomic states, with the exception of 6P are neglected since fluorescence from them is weak. The 6P state is populated by a number of different processes which make it difficult to analyze quantitatively. However, the 6P state is important in our overall picture of the vapor and more will be said about it later. We begin by listing the processes which are considered here. These are also shown schematically in Fig. 1. We then construct rate equations for the relevant populations, solve these for the populations, and hence obtain expressions for the fluorescence ratios.

A. Processes considered

1. Laser excitation of Cs$_2$ molecules

$$Cs_2 + h\nu \rightarrow Cs_2(E). \tag{2}$$

{Here we will use Cs$_2$ and Cs to refer to ground state molecules and atoms, respectively, while Cs$_2(i)$ and Cs(nL) refer to excited molecules and atoms in the states i and nL, respectively. The notation [Cs] will be used for the number density of Cs atoms etc.}
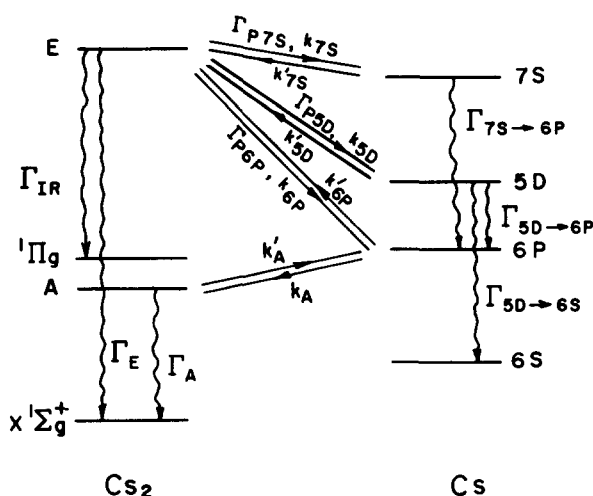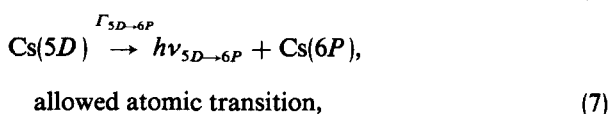
2. Radiative decay

$$Cs_2(E) \xrightarrow{\Gamma_E} h\nu_E + Cs_2, \quad \text{visible } E \text{ band fluorescence,} \tag{3}$$

$$Cs_2(E) \xrightarrow{\Gamma_{IR}} h\nu_{IR} + Cs_2(i), \quad \text{infrared cross fluorescence,} \tag{4}$$

$$Cs_2(A) \xrightarrow{\Gamma_A} h\nu_A + Cs_2, \quad A \text{ band fluorescence,} \tag{5}$$

$$Cs(7S) \xrightarrow{\Gamma_{7S \rightarrow 6P}} h\nu_{7S \rightarrow 6P} + Cs(6P),$$

allowed atomic transition,   (6)

$$Cs(5D) \xrightarrow{\Gamma_{5D \rightarrow 6P}} h\nu_{5D \rightarrow 6P} + Cs(6P),$$
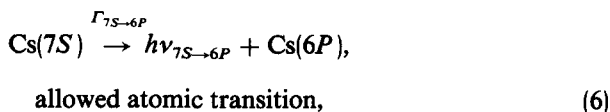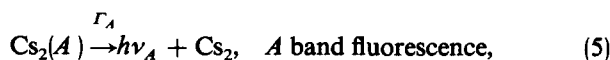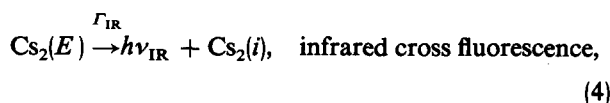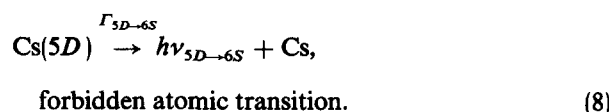
allowed atomic transition,   (7)

FIG. 1. Processes involved in the population and depopulation of cesium atomic and molecular levels in this experiment. Energy levels are not to scale.
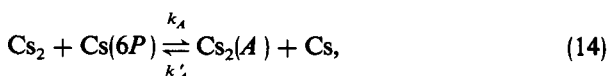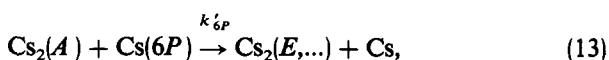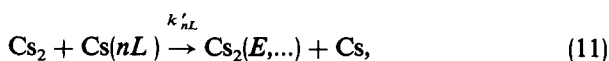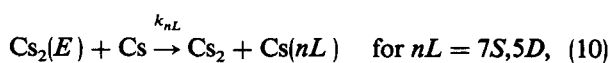
$$Cs(5D) \xrightarrow{\Gamma_{5D \rightarrow 6S}} h\nu_{5D \rightarrow 6S} + Cs,$$

forbidden atomic transition.   (8)

The forbidden transition 5D→6S is included here since it was used to monitor the 5D population as will be discussed below.

3. Predissociation

$$Cs_2(E) \xrightarrow{\Gamma_{PnL}} Cs(nL) + Cs \tag{9}$$

for nL = 7S, 5D, and 6P. All other dissociation limits lie well above the levels pumped by the laser. Note that in our experiment we cannot distinguish predissociation from direct dissociation (i.e., the direct laser pumping of a dissociating state). Additionally, radiation from the E state to dissociating states of the 7S + 6S, 5D + 6S, or 6P + 6S manifolds cannot be distinguished from predissociations in our experiment. Therefore throughout this paper, all reference to "predissociation" must be considered as the sum of predissociation, direct dissociation, and radiation to states dissociating or predissociating to 7S, 5D, or 6P.

4. Collisional excitation transfer between Cs$_2$ and Cs

$$Cs_2(E) + Cs \xrightarrow{k_{nL}} Cs_2 + Cs(nL) \quad \text{for } nL = 7S, 5D, \tag{10}$$

$$Cs_2 + Cs(nL) \xrightarrow{k'_{nL}} Cs_2(E,...) + Cs, \tag{11}$$

$$Cs_2(E) + Cs \xrightarrow{k_{6P}} Cs_2(A) + Cs(6P), \tag{12}$$

$$Cs_2(A) + Cs(6P) \xrightarrow{k'_{6P}} Cs_2(E,...) + Cs, \tag{13}$$

$$Cs_2 + Cs(6P) \underset{k'_A}{\overset{k_A}{\rightleftharpoons}} Cs_2(A) + Cs, \tag{14}$$

where E, ... represents the E state or other nearby states. Because of this back transfer to levels other than those directly populated by the laser, processes (10) and (11) [and (12) and (13)] are not strictly inverses of each other.

Processes such as radiative cascade from atomic levels lying higher than 7S, collisions with impurity gases, and molecule–molecule collisions, are neglected in the rate equation analysis for reasons given in Sec. V C. Experimentally we found almost no radiation from the B $^1\Pi_u$ state. It, and other more highly excited states of the 6P + 6S manifold, were therefore also neglected in this analysis (see Sec. V B).

B. Rate equations

The following rate equations, valid for our steady-state experiment can now be written down:

$$\{d\,[Cs_2(A)]\}/(dt) = 0$$

$$= k_{6P}[Cs_2(E)][Cs] + k_A[Cs_2][Cs(6P)]$$

$$- \{\Gamma_A + k'_{6P}[Cs(6P)] + k'_A[Cs]\}[Cs_2(A)], \tag{15}$$

$$\{d \, [\mathrm{Cs}(7S)]\}/(dt) = 0$$

$$= (\Gamma_{P7S} + k_{7S}[\mathrm{Cs}])[\mathrm{Cs}_2(E)]$$

$$- (\Gamma_{7S \to 6P} + k'_{7S}[\mathrm{Cs}_2])[\mathrm{Cs}(7S)], \qquad (16)$$

and

$$\{d \, [\mathrm{Cs}(5D)]\}/(dt) = 0$$

$$= (\Gamma_{P5D} + k_{5D}[\mathrm{Cs}])[\mathrm{Cs}_2(E)]$$

$$- (\Gamma_{5D} + k'_{5D}[\mathrm{Cs}_2])[\mathrm{Cs}(5D)], \qquad (17)$$

where $\Gamma_{5D} \equiv \Gamma_{5D \to 6P} + \Gamma_{5D \to 6S}$.

These rate equations may be solved to obtain population ratios:

$$\frac{[\mathrm{Cs}(7S)]}{[\mathrm{Cs}_2(E)]} = \frac{\Gamma_{P7S} + k_{7S}[\mathrm{Cs}]}{\Gamma_{7S \to 6P} + k'_{7S}[\mathrm{Cs}_2]}, \qquad (18)$$

$$\frac{[\mathrm{Cs}(5D)]}{[\mathrm{Cs}_2(E)]} = \frac{\Gamma_{P5D} + k_{5D}[\mathrm{Cs}]}{\Gamma_{5D} + k'_{5D}[\mathrm{Cs}_2]}, \qquad (19)$$

$$\frac{[\mathrm{Cs}_2(A)]}{[\mathrm{Cs}_2(E)]} = \frac{k_{6P}[\mathrm{Cs}] + k_A[\mathrm{Cs}_2][\mathrm{Cs}(6P)]/[\mathrm{Cs}_2(E)]}{\Gamma_A + k'_A[\mathrm{Cs}]}, \qquad (20)$$

where in the last expression we have neglected k'_{6P} [Cs(6P)] compared to k'_A [Cs], since [Cs]/[Cs(6P)] ~ 10⁴ (see Sec. V C1) and k'_{6P} cannot be that much larger than k'_A (which will be shown in Sec. V B to be approximately 10^{-9} cm³ s⁻¹).

In this experiment we measured ratios of atomic to visible E band fluorescence given by

$$\frac{I_{nL}}{I_E} = \frac{\Gamma_{nL}}{\Gamma_E} \frac{h\nu_{nL}}{h\nu_E} \frac{\epsilon_{nL}}{\epsilon_E} \frac{[\mathrm{Cs}(nL)]}{[\mathrm{Cs}_2(E)]} \frac{d\Omega_{nL}}{d\Omega_E}, \qquad (21)$$

where the ϵ's are the detection system efficiencies and the $d\Omega$'s are the detection solid angles. We will show in Sec. V A that the back transfer terms, k'_{nL} can be neglected compared to Γ_{nL} in the denominators of Eqs. (18) and (19) for cesium densities less than $\sim 3 \times 10^{16}$ cm⁻³. Therefore we obtain

$$\frac{I_{7S}}{I_E} = \frac{\Gamma_{P7S} + k_{7S}[\mathrm{Cs}]}{\Gamma_E} \frac{h\nu_{7S \to 6P}}{h\nu_E} \frac{\epsilon_{7S \to 6P}}{\epsilon_E} \frac{d\Omega_{7S \to 6P}}{d\Omega_E} \qquad (22)$$

and

$$\frac{I_{5D}}{I_E} = \frac{\Gamma_{5D \to 6S}}{\Gamma_{5D}} \frac{\Gamma_{P5D} + k_{5D}[\mathrm{Cs}]}{\Gamma_E}$$

$$\times \frac{h\nu_{5D \to 6S}}{h\nu_E} \frac{\epsilon_{5D \to 6S}}{\epsilon_E} \frac{d\Omega_{5D \to 6S}}{d\Omega_E}, \qquad (23)$$

where $I_{7S} \equiv I_{7S \to 6P}$ and $I_{5D} \equiv I_{5D \to 6S}$.

It is also clear from the processes considered here that a measurement of the E state lifetime will yield the sum of the rates for its various decay channels

$$1/\tau = \Gamma_T + \sum_{nL} \Gamma_{PnL} + \sum_{nL} k_{nL}[\mathrm{Cs}] + k_u[\mathrm{Cs}], \qquad (24)$$

where Γ_T is the total radiative decay rate of the E state and k_u is the rate coefficient for all other collisional quenching channels that have been neglected in the analysis.

III. FLUORESCENCE MEASUREMENTS

The measurement of the fluorescence ratios was carried out in two steps. First, the density dependencies of I_{7S}/I_E

and I_{5D}/I_E were obtained using the set up shown in Fig. 2(a). This set up eliminated the need for continual switching of detectors to measure I_{7S} and I_E. However, since $d\Omega_{7S \to 6P} \neq d\Omega_E$ in this set up, and since $\epsilon_{7S \to 6P}/\epsilon_E$ was not measured (and we were monitoring only a fraction of the E band fluorescence centered near 5000 Å), these data do not yield absolute values for Γ_{P7S} and k_{7S}. Nevertheless, k_{7S}/Γ_{P7S} is given by the ratio of slope to intercept of the density dependence of I_{7S}/I_E [see Eq. (22)]. Moreover, since $d\Omega_{7S \to 6P} = d\Omega_{5D \to 6S}$, and $\epsilon_{7S \to 6P}/\epsilon_{5D \to 6S}$ was measured (see below), we could also obtain from Eqs. (22) and (23):

$$k_{5D}/\Gamma_{P7S} = \frac{\text{slope of } I_{5D}/I_E}{\text{intercept of } I_{7S}/I_E} \frac{\Gamma_{5D}}{\Gamma_{5D \to 6S}} \frac{\nu_{7S \to 6P}}{\nu_{5D \to 6S}} \frac{\epsilon_{7S \to 6P}}{\epsilon_{5D \to 6S}}$$
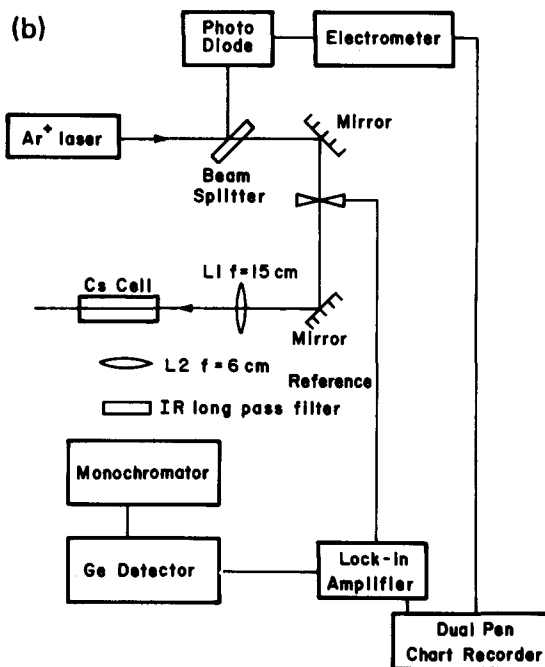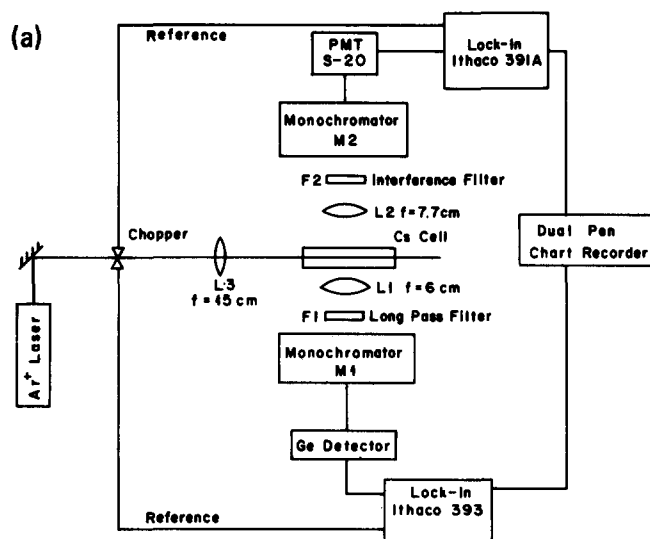
$$\qquad (25)$$

and

(a)

(b)

FIG. 2. (a) Experimental arrangement for measuring density dependencies of I_{7S}/I_E and I_{5D}/I_E; (b) Experimental arrangement for measuring absolute fluorescence ratios.

$\Gamma_{P5D}/\Gamma_{P7S}$

$$= \frac{\text{intercept of } I_{5D}/I_E}{\text{intercept of } I_{7S}/I_E} \frac{\Gamma_{5D}}{\Gamma_{5D\to6S}} \frac{\nu_{7S\to6P}}{\nu_{5D\to6S}} \frac{\epsilon_{7S\to6P}}{\epsilon_{5D\to6S}}. \quad (26)$$

In the second step of the fluorescence measurements, the absolute intensity ratio I_{7S}/I_E was obtained at $[\text{Cs}] = 9.4 \times 10^{15}$ cm^{-3} using the apparatus shown in Fig. 2(b). In this case $d\Omega_{7S\to6P} = d\Omega_E$, and the entire E band fluorescence was measured (as was $\epsilon_{7S\to6P}/\epsilon_E$). We therefore obtained absolute values of $(\Gamma_{P7S}/\Gamma_E)\{1 + (k_{7S}[\text{Cs}])/\Gamma_{P7S}\}$ [see Eq. (22)] where the quantity in curly brackets was known from the first step. Γ_E was obtained from the lifetime measurements described in the next section. Thus absolute values of Γ_{P7S}, k_{7S}, Γ_{P5D}, and k_{5D} could be determined.

The cylindrical cells, 2.54 cm in diameter and 20 cm long, were in all cases made of aluminosilicate glass (Corning 1720). They were baked at about 600 °C for 12 h in a vacuum of $\sim 10^{-6}$ Torr before a small amount of Cs metal (99.9% pure) was distilled into them and they were sealed off. During the experiment, the cell was heated to between 200 and 375 °C in a glass oven using Nichrome wire heaters. The temperature of the cell was monitored by a chromel–alumel thermocouple attached to the cell tip where the small pool of liquid Cs metal sat. The thermocouple was covered with ceramic cement which shielded it from direct radiation from the Nichrome heaters which otherwise can give incorrect temperature readings. The Cs vapor pressure as a function of temperature was determined as described in Sec. V C4.

The Cs vapor was excited by the fixed frequency lines 465.8, 488.0, and 514.5 nm of the argon ion laser (Spectra-Physics model 171) focused to an ~ 0.35 mm beam diameter. Laser power was typically 200 mW at the cell. In step one, fluorescence was focused onto the slits of the monochromators M1 and M2 in Fig. 2(a) (0.3 m McPherson model 218) with the imaging systems aligned so that the same spatial region of the cell was observed in both channels. The long pass filter in front of M1, which was used to eliminate second and higher order grating effects, was either Schott RG715 or RG590 for observation of the 7S or 5D fluorescence, respectively. The slits of M1 were both set at 150 μm which corresponds to a resolution of 0.8 nm. The infrared $7S\to6P_{3/2}$ fluorescence at $\lambda = 1.47$ μm was detected by an intrinsic germanium detector (North Coast model EO-917L) whose output was amplified by a lock-in detector (Ithaco model 393) and displayed on a chart recorder. Note that in practice we obtained I_{7S} from the relation $I_{7S} = I_{7S\to6P_{3/2}}/\gamma_{7S\to6P_{3/2}}$, where $\gamma_{7S\to6P_{3/2}}$ is the branching ratio $\Gamma_{7S\to6P_{3/2}}/\Gamma_{7S\to6P}$. This was necessary since the $7S\to6P_{1/2}$ fluorescence at 1.36 μm is overlapped by the weak $7P_{3/2}\to5D_{5/2}$ line. For observation of the $5D\to6S$ fluorescence at $\lambda = 685.1$ and 689.8 nm, the Ge detector was replaced by a photomultiplier (Hamamatsu R928 with -700 V cathode bias), and the 1.6 μm blazed grating used in M1 for the 7S measurements was replaced by one blazed at 750 nm (resolution 0.4 nm for 150 μm slits).

In the channel detecting the molecular fluorescence, M2 was set to a wavelength of 500 nm and both slits were

opened to 600 μm (1.4 nm resolution). The interference filter has a 6 nm FWHM bandpass centered on 500 nm. The combination of filter and monochromator was necessary to reduce the contribution of scattered laser light to the molecular fluorescence signal to $\sim 0.1\%$. The molecular fluorescence was detected by a photomultiplier (EMI 9558, S-20 cathode response, -700 V cathode bias) terminated in 10^5 Ω, whose output was amplified by a lock-in detector (Ithaco model 391A) and displayed on the second channel of the chart recorder.

The relative detection system efficiency at the 7S and 5D wavelengths, $\epsilon_{7S\to6P}/\epsilon_{5D\to6S}$, which includes effects of the lens L1, and the different long pass filters, gratings, monochromator settings, and detectors, was obtained using a standard blackbody source (Infrared Industries model 463) with known relative emission at the two wavelengths. Details of this calibration are given in Ref. 13 where we obtained $\epsilon_{7S\to6P}/\epsilon_{5D\to6S} = 3.73 \pm 15\%$.

We chose to monitor the $5D\to6S$ forbidden transition rather than the allowed $5D\to6P$ transition at $\lambda \sim 3$ μm, since the latter would require special optics and detectors. Additionally, despite the small oscillator strength of the $5D\to6S$ line, the greatly improved signal to noise ratios of photomultipliers working in the visible compared to the best detectors at 3 μm (PbS), indicate that the $5D\to6P$ signal would not be significantly enhanced over the $5D\to6S$ signal. Nevertheless, observation of this forbidden line resulted in the introduction of the branching ratio $\Gamma_{5D\to6S}/\Gamma_{5D}$ in Eq. (23) which leads to several possible sources of systematic error. In particular, radiation trapping of $5D\to6P$ or $5D\to6S$ fluorescence, collision-assisted $5D\to6S$ fluorescence, and uncertainties in the branching ratio itself must be considered. Discussions of these effects are given in Sec. V.

The absolute intensity ratio measurements I_{7S}/I_E and I_{IR}/I_E were obtained using the experimental arrangement of Fig. 2(b). Here I_{IR} is the intensity of the infrared cross fluorescence between 1.48 and 1.65 μm (Refs. 6–8). Assuming that emission with $\lambda > 1.8$ μm makes a negligible contribution to the total infrared emission (see Sec. V C 6), we obtain the E state infrared branching ratio γ_{IR} from

$$\gamma_{IR} \equiv \frac{\Gamma_{IR}}{\Gamma_{IR} + \Gamma_E} = \{ [I_E\epsilon_{IR}\lambda_E/(I_{IR}\epsilon_E\lambda_{IR})] + 1 \}^{-1}.$$

$$(27)$$

In these measurements I_{IR} and I_{7S} were obtained using the Ge detector, 1.6 μm blazed grating and Schott RG850 long pass filter, while I_E was obtained with the Hamamatsu R928 PMT, 750 nm blazed grating and WG345 long pass filter. In this case, no interference filter was used, and the entire band spectra were scanned, thereby obtaining the full band intensities (spectrally integrated with a planimeter). Calibration of the relative light detection efficiency, as a function of wavelength, was obtained using the blackbody source (details of the calibration may be found in Ref. 13).

IV. LIFETIME MEASUREMENTS

Measurements of the Cs₂(E) state lifetime as a function of Cs density and for the three excitation wavlengths 465.8, 488.0, and 514.5 nm were made using the phase shift tech-

nique.[9,14–16] These measurements are similar to those of Baumgartner *et al.*[9] However, in that earlier experiment, the vapor pressure was given only in arbitrary units and therefore the collisional depopulation rate coefficients are not available. Also, except for 488.0 nm, the excitation wavelengths used here are different from those of Ref. 9. Comparison of the results of these two experiments is given in Sec. VI.

In the phase shift technique, the vapor is excited by a sinusoidally modulated laser beam. Since the fluorescence from excited atoms or molecules decays according to $\exp(-t/\tau)$ with τ the upper state lifetime, it can be shown (see Ref. 13) that the fluorescence signal will be modulated at the same frequencies as the laser. However, due to the finite lifetime τ, each frequency component in the fluorescence will lag the corresponding component ω_n in the laser by a phase angle ϕ_n given by

$$\tan \phi_n = \omega_n \tau. \tag{28}$$

Figure 3 shows the experimental arrangement for the lifetime measurements. The acousto–optic light modulator (Intra Action model AOM-110) operates on a 110 MHz acoustic carrier wave, generated by the rf driver, which is amplitude modulated at up to 20 MHz with the video input. For incident power of ~ 240 mW from the argon ion laser (Spectra-Physics model 171) we obtained ~ 80 mW modulated power in the first order Bragg scattered beam. The cesium cell and oven were the same as used in the fluorescence measurements. Molecular fluorescence was focused onto the PMT (RCA 1P28, spectral response S-5, cathode bias -900 V) which was carefully masked and covered by the 6 nm FWHM interference filter with bandpass central wavelength of 500 nm. This reduced the contribution to the E band fluorescence signal from laser scatter to less than 4% and also eliminated other unwanted atomic and molecular fluorescence. The PMT anode rise time is approximately 2.4 ns but this does not affect our results significantly. The out-

put of the PMT was sent to a preamplifier (PAR model 115, 0–70 MHz bandwidth) and then to a high frequency lock-in amplifier (PAR model 5202) which provided simultaneous in-phase and quadrature readouts.

The phase of the excitation source was determined by replacing the cell with a ground quartz diffuser, being careful not to change the path length from modulator to detector (although even a 30 cm path difference would only introduce a 1 ns delay). The laser light was scattered onto the diffuser by passing through another ground quartz plate so that uniform illumination of the PMT window was achieved. The PMT mask was such, however, that the same part of the PMT cathode was illuminated by both the fluorescence and laser scatter to avoid problems associated with different electron transit times from different cathode regions. Quartz was chosen for the diffusers because of its low absorption of visible light which guaranteed that the scattered light was instantaneous (i.e., that no additional phase shifts were introduced by the diffusers). The intensity of the scattered light was sufficiently high that the interference filter could be left in place to act as an attenuator, thereby eliminating any extra phase shifts due to its use in only one step of the measurements.

In the experiment, the laser scatter was observed and the lock-in adjusted to read entirely "in-phase". The diffusers were then replaced by the cell and the ratio of the quadrature to in-phase signals I_q/I_p was read directly, thus yielding $\tan \phi$ and therefore the lifetime

$$I_q/I_p = \tan \phi = \omega_m \tau. \tag{29}$$

Typically the modulation frequency $\omega_m/2\pi$ was 3 MHz. However, we verified that $\tan \phi$ scales linearly with ω (see Fig. 4), which is as expected if the levels whose radiation we detect for a given laser wavelength all have approximately the same lifetime.

V. RESULTS

A. Fluorescence measurements

Figure 5 is a plot of I_{7S}/I_E and I_{5D}/I_E vs cesium density for excitation at 514.5 nm. At low density the I_{7S}/I_E data are well fitted by a straight line whose slope to intercept ratio is k_{7S}/Γ_{P7S} [see Eq. (22)]. At higher densities the curve turns over due to the back transfer term k'_{7S} in Eq. (18). Unfortunately, we cannot use these data to obtain the back transfer rate coefficients since the high density region of the curve is also affected by impurity gas effects (see Sec. V C5).

In Table I we present the ratios k_{7S}/Γ_{P7S}, k_{5D}/Γ_{P7S}, and $\Gamma_{P5D}/\Gamma_{P7S}$ obtained from these relative fluorescence measurements.

The absolute intensity ratios I_{7S}/I_E were measured at $[Cs] = 9.4 \times 10^{15}$ cm^{-3}. In this case, the detection solid angle was the same for the atomic 7S and molecular E band fluorescence [see Eq. (22)] and $\epsilon_{7S \to 6P}/\epsilon_E = 16.4 \pm 15\%$. The values of Γ_{P7S}/Γ_E thus obtained from these data and Eq. (22) are also given in Table I. Γ_E is related to the total radiative rate of the E state, $\Gamma_T \equiv \Gamma_E + \Gamma_{IR}$, by the visible fluorescence branching ratio $(1 - \gamma_{IR})$:

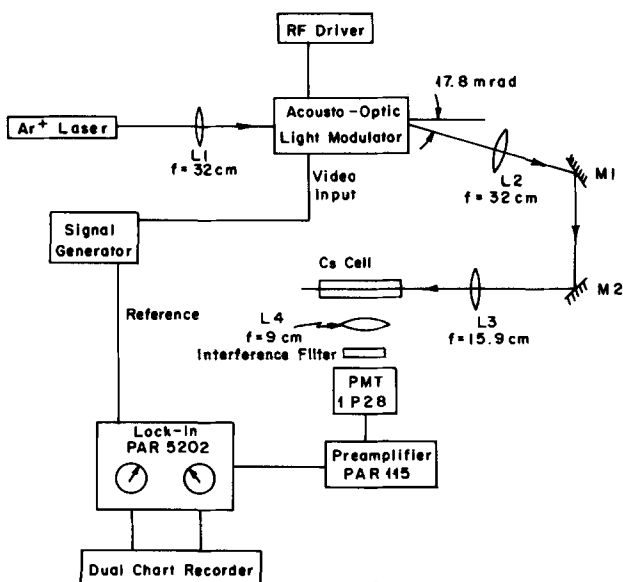$$\Gamma_E = \Gamma_T(1 - \gamma_{IR}). \tag{30}$$

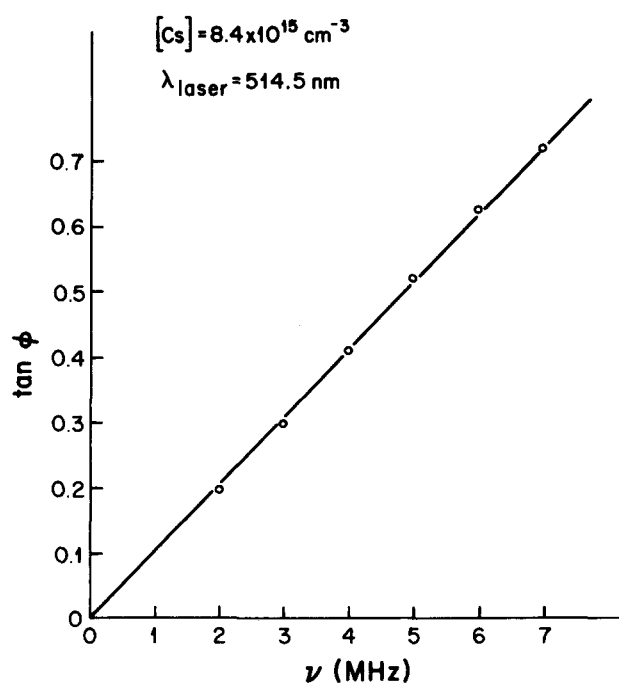FIG. 3. Experimental arrangement for the lifetime measurements.

FIG. 4. Tangent of the phase shift in the lifetime measurements vs modulation frequency [see Eq. (29)].

Γ_E was then obtained from the zero density intercept of the $1/\tau$ curve (see Sec. V B) and thus the absolute values of Γ_{P7S}, k_{7S}, Γ_{P5D}, and k_{5D} were obtained. These are listed in Table II. Note that since we measured the fluorescence from $5D_{5/2}$ and $5D_{3/2}$ separately, and since little collisional mixing was taking place (see Sec. V C.12), we could also determine the values of $\Gamma_{P5D_{5/2}}$ and $\Gamma_{P5D_{3/2}}$ individually. These are also given in Table II. The large uncertainties in the k_{5D} values made such a separation meaningless in that case, however.

B. Lifetime measurements

Figure 6 shows a plot of $1/\tau$ vs Cs density for vapor excited by the 514.5 nm argon ion line. The data are well represented by a straight line. From Eq. (24) we see that the slope of the line is given by $\Sigma_{nL} k_{nL} + k_u$ while the zero density intercept τ_E is given by

$$\frac{1}{\tau_E} = \Gamma_E + \Gamma_{IR} + \sum_{nL} \Gamma_{PnL}$$

$$= \Gamma_E \left[1 + \frac{\gamma_{IR}}{1 - \gamma_{IR}} + \frac{\Gamma_{P7S}}{\Gamma_E} \left(1 + \frac{\Gamma_{P5D}}{\Gamma_{P7S}} + \frac{\Gamma_{P6P}}{\Gamma_{P7S}} \right) \right].$$

(31)

Measured values for τ_E are given in Table III. The branching ratio γ_{IR} was obtained from the visible to infrared E state fluorescence ratio [see Eq. (27)], and these values are also given in Table III. $\Gamma_{P5D}/\Gamma_{P7S}$ and Γ_{P7S}/Γ_E were taken from Table I. The term $\Gamma_{P6P}/\Gamma_{P7S}$ was neglected compared to $\Gamma_{P5D}/\Gamma_{P7S}$ in our analysis. The data of Collins et al.[10–12] for prompt photolysis indicated that $(\Gamma_{P6P} + k_{6P}[Cs])/(\Gamma_{P5D} + k_{5D}[Cs]) \sim 0.05$ at their Cs density of 2.14×10^{15} cm^{-3}. Because of the different time scales of the Collins et al. experiment and the present work [where delayed photolytic processes may contribute (see Sec. VI)], this value is not in-
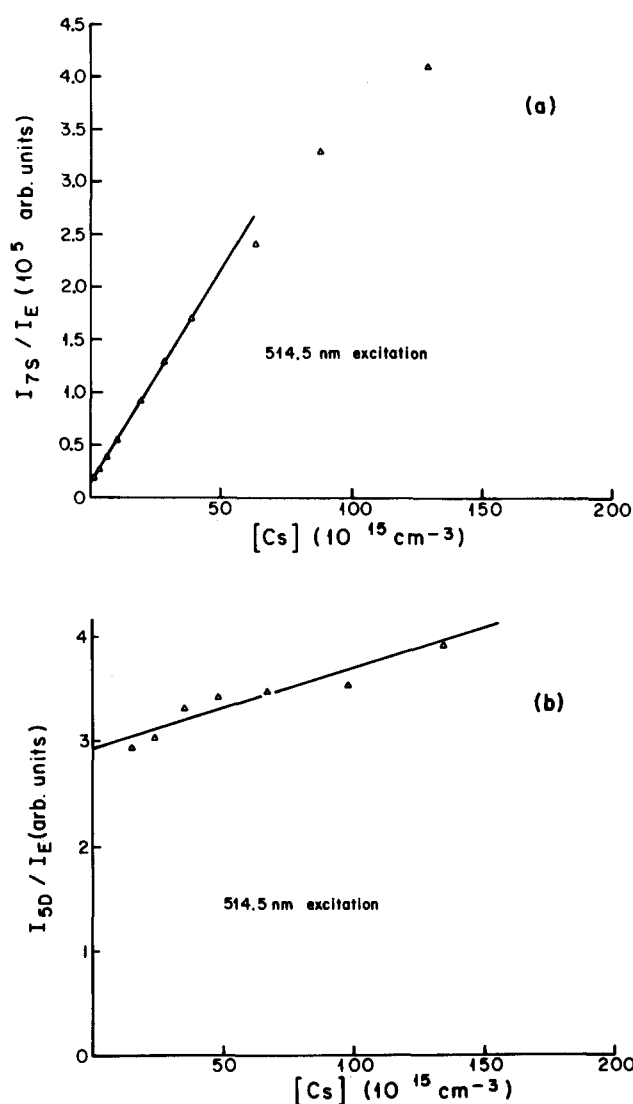

FIG. 5. (a) I_{7S}/I_E and (b) I_{5D}/I_E vs [Cs] for 514.5 nm excitation. Arbitrary units are the same for both figures.
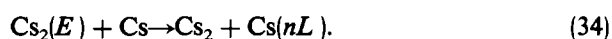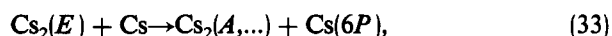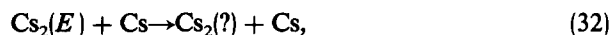
consistent with our values of Γ_{P5D}, k_{5D}, and k_{6P} (see Tables II and III) which yield $k_{6P}[Cs]/(\Gamma_{P5D} + k_{5D}[Cs]) \sim 0.5$ at $[Cs] = 2.14 \times 10^{15}$ cm^{-3}. The Collins result implies $\Gamma_{P6P}/\Gamma_{P5D} < 0.05$. Even with the possibility of contributions from delayed processes in our cw experiment we believe it is safe to assume that $\Gamma_{P6P}/\Gamma_{P5D} < 0.5$ in our case and is most likely much less. The maximum uncertainty in Γ_E due to neglect of Γ_{P6P} in Eq. (31) is therefore 25%. Values of Γ_E obtained from Eq. (31) and of Γ_T from Eq. (30) are presented in Table III.

The slopes of the $1/\tau$ curves represent the total collisional quenching rates of the Cs$_2(E)$ state by ground state Cs atoms. We designate these total quenching rates as k_E and their measured values are given in Table III. From Eq. (24) we see that $k_E = k_{5D} + k_{7S} + k_{6P} + k_u$, where k_{5D} and k_{7S} are known and k_{6P} and k_u are not. It can be seen from Tables II and III that k_E is much greater than $k_{5D} + k_{7S}$. Therefore either k_{6P} or some unknown collisional depopulation mechanism dominates k_E. The straight line dependence of $1/\tau$ on density indicates that this quenching is due to collisions with ground state atoms. We may identify three types of depopu-

TABLE I. Ratios of various rates and rate coefficients obtained from the data and Eqs. (22), (23), (25), and (26). See the text for definitions.

λ_{laser} (nm)	k_{7S}/Γ_{P7S} (cm^3)	k_{5D}/Γ_{P7S} (cm^3)	$\Gamma_{P5D}/\Gamma_{P7S}$	Γ_{P7S}/Γ_E
514.5	$4.2\times10^{-16}\pm30\%$	$<12\times10^{-17}$	$17\pm50\%$	$0.11\pm15\%$
488.0	$3.0\times10^{-16}\pm30\%$	$<6\times10^{-17}$	$18\pm50\%$	$0.17\pm15\%$
465.8	$1.1\times10^{-16}\pm30\%$	$<2\times10^{-18}$	$0.68\pm50\%$	$7.4\pm15\%$

lating collisions between Cs$_2$(E) molecules and ground state atoms based on energetics. They are represented by the following equations:

$$Cs_2(E) + Cs \rightarrow Cs_2(?) + Cs, \qquad (32)$$

$$Cs_2(E) + Cs \rightarrow Cs_2(A,...) + Cs(6P), \qquad (33)$$

$$Cs_2(E) + Cs \rightarrow Cs_2 + Cs(nL). \qquad (34)$$

Process (34) by which the 7S and 5D states are populated has already been discussed and the rate coefficients determined. In Sec. V C8 we will show that no states higher than 7S are significantly populated by process (34).

Process (32) in which the atom remains in the ground state but the molecule changes state is certainly possible and indeed must occur. In fact it is clear that our analysis of the E state here is really an analysis of the state or states populated by the various laser lines and by such collisions. For instance, collisions that mix different vibrational states must occur although we see no obvious density dependence to the intensity distribution of the E band fluorescence spectrum. Any collisionally populated state which radiates at the visible E band or infrared cross fluorescence band wavelengths is lumped with the E state for the purposes of our analysis. By demonstrating that γ_{IR} is independent of density, we found that the observed IR cross fluorescence is radiation from directly excited levels rather than from collisionally populated states. We have made a careful check for other molecular fluorescence (besides the visible and infrared E state fluorescence and the A band fluorescence) at wavelengths between 0.4 and 1.8 μm. No additional molecular radiation with significant intensity was found. It is possible, however, that a collisionally populated state could cascade back to the ground state, emitting photons with $\lambda > 1.8\,\mu$m. This will be discussed further in Sec. V C6.

The processes represented by Eq. (33) are very interesting since both the molecule and the atom end up in excited states after the collision. From a consideration of the energetics of the situation it is clear that the only excited atomic state that would permit simultaneous excitation of the molecule is the 6P state. Additionally, the final molecular state must be in the 6P + 6S manifold and in fact we can demonstrate that the only states in this manifold that would be significantly populated in this manner are the $a\,^3\Pi_u$, $A\,^1\Sigma_u^+$, and $b\,^3\Sigma_g^+$. (This is confirmed by the absence of any significant $B\,^1\Pi_u$ band emission in our spectra.) These states only radiate in the near infrared on the following transitions $a\,^3\Pi_u \rightarrow X\,^1\Sigma_g^+$, $A\,^1\Sigma_u^+ \rightarrow X\,^1\Sigma_g^+$, and $b\,^3\Sigma_g^+ \rightarrow x\,^3\Sigma_u^+$, since the $\Delta S = 0$ selection rule is easily broken for the massive Cs$_2$ molecule while the selection rule $g \leftrightarrow u$ remains in effect. In fact the transition wavelengths of these three bands overlap to such a degree that they cannot be distinguished. As mentioned previously, we lump them together in what we call A band emission I_A.

The value of k_{6P} can be determined crudely by measuring the relative values of I_A/I_E at several densities, and the absolute value at one density. From Eq. (20) we find:

$$\frac{I_A}{I_E} = \frac{k_{6P}[Cs] + k_A(V_{6P}/V_E)[Cs_2][Cs(6P)]/[Cs_2(E)]}{\Gamma_E[1 + (k'_A\,[Cs]/\Gamma_A)]}$$

$$\times \frac{\nu_A}{\nu_E}\frac{\epsilon_A}{\epsilon_E}, \qquad (35)$$

where (V_{6P}/V_E) is the ratio of the effective volumes occupied by 6P atoms and E state molecules (which are not equal due to radiation trapping effects), and $[Cs(6P)]/[Cs_2(E)]$ is obtained from

$$\frac{[Cs(6P)]}{[Cs_2(E)]} = \frac{I_{6P}}{I_E}\frac{\Gamma_E}{\Gamma_{6P\rightarrow6S}^{eff}}\frac{\nu_E}{\nu_{6P\rightarrow6S}}\frac{\epsilon_E}{\epsilon_{6P\rightarrow6S}}\frac{V_E}{V_{6P}}, \qquad (36)$$

where $\Gamma_{6P\rightarrow6S}^{eff}$ is the effective radiative decay rate of the 6P level due to radiation trapping, which we calculate from Holstein's theory.[17,18] Since [Cs] and [Cs$_2$] have different dependencies on temperature,[19] the relative importance of the various terms in both numerator and denominator of Eq. (35) changes with temperature. If the second term in the nu-

TABLE II. Values of predissociation rates and collisional excitation transfer rate coefficients determined in this experiment. See the text for definitions.

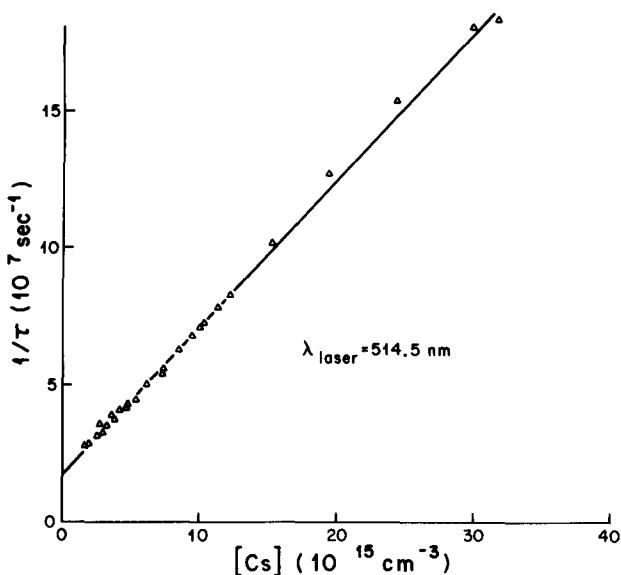| Excitation wavelength (nm)	Γ_{P7S} (s^{-1})	k_{7S} (cm^3 s^{-1})	$\Gamma_{P5D_{3/2}}$ (s^{-1})	$\Gamma_{P5D_{5/2}}$ (s^{-1})	Γ_{P5D} (s^{-1})	k_{5D} (cm^3 s^{-1})
514.5	5.0×10^5 $\pm45\%$	2.1×10^{-10} $\pm55\%$	4.9×10^6 $\pm65\%$	3.6×10^6 $\pm65\%$	8.5×10^6 $\pm65\%$	$<6\times10^{-11}$
488.0	8.5×10^5 $\pm45\%$	2.6×10^{-10} $\pm55\%$	8.8×10^6 $\pm65\%$	6.4×10^6 $\pm65\%$	1.5×10^7 $\pm65\%$	$<5\times10^{-11}$
465.8	2.0×10^7 $\pm45\%$	2.2×10^{-9} $\pm55\%$	7.8×10^6 $\pm65\%$	5.6×10^6 $\pm65\%$	1.3×10^7 $\pm65\%$	$<4\times10^{-11}$

FIG. 6. $1/\tau$ vs [Cs] for 514.5 nm excitation, where τ is the $Cs_2(E)$ state lifetime.

merator of expression (35) were dominant over the first, the value of k_{6P} would be too small to explain the observed $6P$ density (see below). Thus we neglect the second term and fit Eq. (35) to the data to obtain values of k_{6P} and k'_A. The values of k_{6P} determined in this manner are listed in Table III where it can be seen that they agree with the total quenching rates to within a factor of 2 or 3 but are uncertain by about the same amount. This is consistent with our determinations of [Cs(6P)] [see Eq. (36) and Sec. V C1] which indicate that between 40% and 80% of absorbed photons eventually result in excitation of $6P$. This in turn requires that a large fraction of the total E state collisional quenching results in excitation of $6P$. Thus our data is consistent with $k_E = \Sigma_{nL} k_{nL}$ but is uncertain to such a degree that we cannot rule out a large but unknown quenching rate coefficient k_u as in Eq. (24).

Using $\Gamma_A \sim 3 \times 10^7$ s^{-1}, which is the atomic value, we also obtained $k'_A = 1.1 \times 10^{-9}$ cm^3 s^{-1} from the fit which is consistent with values measured for analogous rates in sodium and potassium.[20-22] Assuming $k_A \sim k'_A$ we calculate that, in the worst case, the neglected term in the numerator of Eq. (35) is on the order of 50% of the first term. Thus it can be seen that the determinations of k_{6P} and k'_A are indeed only good to within a factor of 2 or 3.

We note that Baumgartner et al.[9] indicated that the main collisional depopulation channel for the Cs_2 (E) state is

excitation transfer to the B, C, and D states. However, we see no significant fluorescence from any of these states.

C. Additional considerations and sources of uncertainty

1. Radiation trapping

Trapping of resonance radiation at the high optical depths of this experiment is a well known phenomenon, which leads to greatly reduced radiative decay rates for the resonance $6P$ state. This bottlenecking at $6P$ causes substantial populations to build up in that state which may result in trapping of the $7S \rightarrow 6P$ and $5D \rightarrow 6P$ atomic fluorescences, and thereby influence our results. In fact, as can be seen from Eq. (22), valid in the low density (linear) region, trapping of $7S \rightarrow 6P$ fluorescence can not significantly affect our results for k_{7S} and Γ_{P7S} since $\Gamma_{7S \rightarrow 6P}$ does not appear in the expression for the fluorescence ratio. However, trapping of $7S \rightarrow 6P$ would affect an attempt to determine the back transfer rate coefficient k'_{7S} since k'_{7S} [Cs_2] competes with $\Gamma_{7S \rightarrow 6P}$ in Eq. (18). Trapping of $5D \rightarrow 6P$ or $5D \rightarrow 6S$ fluorescence, on the other hand, would affect our results for k_{5D} and Γ_{P5D}, even in the linear region, through its effect on the branching ratio $\Gamma_{5D \rightarrow 6S}/\Gamma_{5D}$. In order to estimate the magnitude of these effects, we need to know the steady state $6P$ density which we can roughly determine from I_{6P}/I_E as in Eq. (36). The $Cs_2(E)$ state density is simply given by

$$[Cs_2(E)] = P\tau, \qquad (37)$$

where P is the laser pumping rate (photons absorbed/cm^3 s) and τ is the E state lifetime determined as in Sec. IV. $\Gamma^{\text{eff}}_{6P \rightarrow 6S}$ in Eq. (36) was calculated using Holstein's theory[17,18] and the cesium self-broadening rates from Carrington et al.[23] V_E/V_{6P} was obtained from the square of the ratio of the laser beam diameter, 0.35 mm, to the diameter of the column of excited $(6P)$ atoms, 1.2 mm, which was measured by spatial resolution of the $6P$ fluorescence. The $6P$ density obtained in this way was typically $(1-5) \times 10^{11}$ cm^{-3}. We then calculated k_0, the line center absorption coefficient (see Ref. 24), for each $5D \rightarrow 6P$ and $7S \rightarrow 6P$ fine structure component, and from that, $\bar{k}l$ where $\bar{k}$ is an effective absorption coefficient, averaged over the line profile, which was calculated from Samson's equivalent opacity.[24] Here $l \sim 0.6$ mm represents the spatial extent (radius of cylinder) of the absorbing $6P$ atoms. We then calculated the escape factor $g \equiv \Gamma^{\text{eff}}/\Gamma^{\text{nat}}$ from Milne's theory of radiation trapping[25] which has been shown to be valid in this optical density range.[26] Similarly we calculated trapping of the forbidden $5D \rightarrow 6S$ fluorescence

TABLE III. $Cs_2(E)$ state lifetimes, radiative rates, branching ratios, and collisional quenching rate coefficients, and the rate coefficients for process (12) determined in this experiment.

Excitation wavelength (nm)	τ_E(ns)	Γ_T(s^{-1})	Γ_E(s^{-1})	γ_{IR}	k_E(cm^3 s^{-1})	k_{6P}(cm^{3}s^{-1})
514.5	59 ± 20%	8.0×10^6	4.4×10^6	0.45	5.5×10^{-9}	$(2.0^{+2.0}_{-1.0}) \times 10^{-9}$
		± 50%	± 45%	± 20%	± 30%	
488.0	42 ± 20%	7.7×10^6	5.0×10^6	0.35	6.1×10^{-9}	$(3.4^{+3.4}_{-1.7}) \times 10^{-9}$
		± 50%	± 45%	± 20%	± 30%	
465.8	28 ± 20%	2.7×10^6	2.7×10^6	~ 0	1.7×10^{-8}	$(5.5^{+5.5}_{-2.8}) \times 10^{-9}$
		± 50%	± 45%		± 30%	

which was not entirely negligible due to the large ground state atom density and large effective l. We were then able to calculate $5D$ branching ratios vs density which included these effects of radiation trapping. For $[Cs] < 3 \times 10^{16}$ cm^{-3}, the branching ratio was affected by $\sim 30\%$ in the worst case. In most cases, the effects were much less. Trapping of the molecular E band fluorescence was also considered and found to be negligible in all cases.

Trapping of $5D \rightarrow 6P$ and $7S \rightarrow 6P$ fluorescence can also be demonstrated to be insignificant by considering the dependencies of I_E, I_{6P}, I_{7S}, and I_{5D} on laser intensity. All of these dependencies were equal [and almost linear (see Sec. V C.9)] within experimental uncertainties. Effects of trapping of $5D \rightarrow 6P$ and $7S \rightarrow 6P$ fluorescence are expected to be more severe at high intensities where $[Cs(6P)]$ is largest. However, no such effects on I_{5D}/I_E and I_{7S}/I_E were seen.

An additional effect of radiation trapping must also be considered. Since the slope of I_{5D}/I_E is so small (see Fig. 5), minor trapping corrections could influence k_{5D} significantly. The values of k_{5D} listed in Table II are upper limits obtained when trapping was neglected. However, these values may be greatly in error if the trapping effects were actually more severe than our estimate.

The other results presented in Tables II and III, including Γ_{P7S}, Γ_{P5D}, k_{7S}, and Γ_E, are not in error by more than $\sim 10\%$ due to radiation trapping effects, according to our analysis.

2. Collision assisted radiation

Since we were observing a forbidden transition $5D \rightarrow 6S$ the branching ratio $\Gamma_{5D \rightarrow 6S}/\Gamma_{5D}$ could be seriously affected by fully allowed collision-assisted radiation from quasimolecular states. In fact, as seen in Fig. 7, broad molecular fluorescence bands do appear underneath the forbidden atomic lines at high density. These bands have been studied at high resolution by Niemax[27] who identified them as the quasistatic wings of the forbidden lines with a transition probability at least three orders of magnitude larger than the collision-free atomic lines. Fortunately most of this radiation is shifted in frequency away from the atomic lines and outside the resolution of the monochromator. We obtained atomic line intensities by measuring the peak heights excluding this quasimolecular background. Figure 5(b) shows that $I_{5D \rightarrow 6S}/I_E$ determined in this way is not seriously affected by collision-assisted radiation (which must scale at least linearly with $[Cs]$) since the part of $I_{5D \rightarrow 6S}/I_E$ which scales linearly with $[Cs]$ is small compared to the part which is independent of density. However, the additional uncertainty in measuring $5D$ peak heights due to this background is a major cause of uncertainty in our attempts to determine values for k_{5D}.

3. 5D branching

Uncertainty in the values of the Einstein A coefficients used here will also contribute to the systematic error in the $5D$ branching ratio. In our analysis we took all A coefficients from Warner.[28] Niemax[27] found Warner's values for the forbidden line oscillator strengths agree with experiment to within 30%. These values also agree with the experimental results of Exton[29] and Sayer et al.[30] but differ by much larger
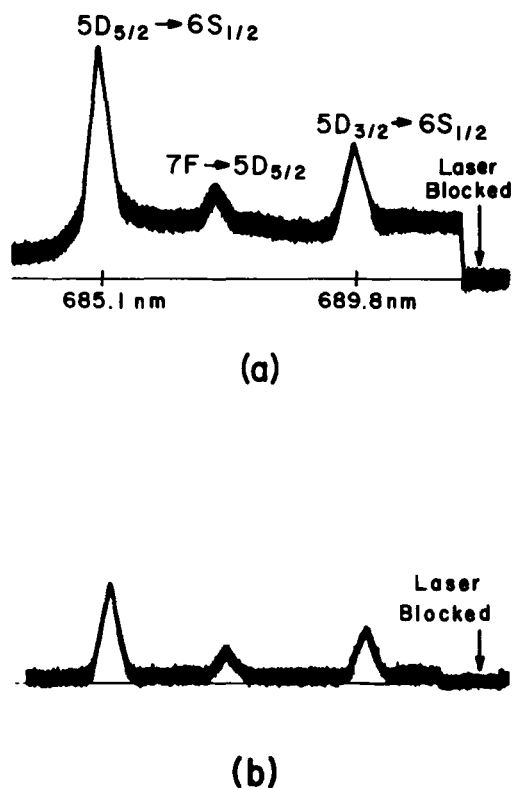

FIG. 7. Cesium $5D \rightarrow 6S$ fluorescence for excitation at 488.0 nm (a) $T = 376$ °C (b) $T = 277$ °C. Note the molecular fluorescence bands which appear in the high temperature scan.

factors with earlier experimental[31-33] results. We therefore estimate an uncertainty of $\sim 30\%$ in our $5D$ results due to this cause.

4. Ground state atom density

Use of a vapor pressure curve such as Nesmeyanov's[19] to obtain the ground state atom density can lead to significant systematic errors in experiments such as this where collisional rate coeffficients are determined. Uncertainty occurs not only in the vapor pressure curve itself, but also in the temperature measurement, and in the failure to sample the temperature at the coldest point in the cell, etc.

To minimize such systematic errors in this experiment, we measured the ground state atom density directly using the equivalent width technique. For the densities of this experiment $10^{15} < [Cs] < 10^{17}$ cm^{-3}, the equivalent width depends strongly on the self-broadening rate which we took from the calculations of Carrington et al.[23] Those values were recently verified in Na to within experimental uncertainties of 15%.[34] All densities used in our analysis are based on these equivalent width measurements which systematically fall $\sim 30\%$ below those obtained from the Nesmeyanov vapor pressure formula. We use this discrepancy as an estimate of the uncertainty in the density determination.

Ground state Cs$_2$ densities were taken from Nesmeyanov's formula[19] and ranged from 3.3×10^{12} to 2.4×10^{15} for $T = 200$–375 °C. These values do not significantly affect any of the rate coefficients determined in this experiment.

5. Impurity gases

Impurity gases, especially diatomic molecules such as H_2 or N_2, could influence our results by quenching excited atoms and molecules and by contributing to collisional transfer rates. Two distinct types of impurity gas are present in our cells. The first is in the gas phase even at low temperatures and therefore the number density of such an impurity is independent of temperature. This type of impurity affects the zero density intercept, but not the slope, of $1/\tau$ in the lifetime measurements. Lifetime measurements using 488.0 nm excitation were carried out in two cells baked out on the vacuum system prior to filling at 580 and 650 °C, respectively. The values of τ_E obtained in these two cells were 33.9 and 42.2 ns with the larger value being associated with the 650 °C cell. We cannot guarantee that all such impurities were baked out of the 650 °C cell, but we report values taken from that cell and use the discrepancy in τ_E from the two cells (~20%) as an estimate of the uncertainty due to these impurities.

A second type of impurity rapidly increases in concentration as the cell temperature increases. The most likely such impurity is H_2 which is released from the breakup of CsH and perhaps also from glass walls. The vapor pressure of such a gas can be several orders of magnitude greater than that of Cs_2.[35] These impurities could quench $7S$ atoms and therefore an impurity gas quenching term should appear in the denominator of Eq. (18) where it would compete with the back transfer term k'_{7S} [Cs_2]. Figure 8 shows relative fluorescence measurements I_{7S}/I_E obtained with three cells baked out at different temperatures prior to filling. Due to different geometries, etc., the three data sets were normalized to unit intercept for comparison purposes, since only the slope to intercept ratio is of significance. As can be seen in the figure, the low density slope to intercept ratio, upon which the $\Gamma_{P_{nL}}$'s and k_{nL}'s were based, is independent of the cell. The high density data, however, vary significantly from cell to
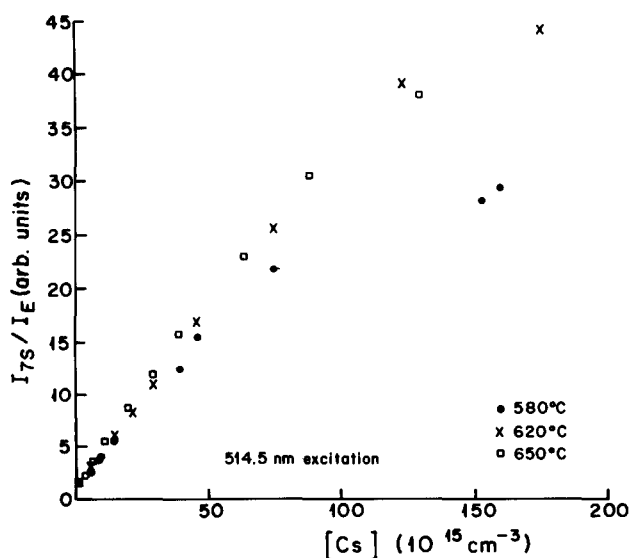

FIG. 8. Fluorescence ratio I_{7S}/I_E vs [Cs] for three cells baked at different temperatures prior to filling. Due to different geometries, etc., the results are normalized to unit intercept for comparison purposes since only the slope to intercept ratio is significant.

cell, indicating that for these temperatures, impurity gas quenching is important. Thus we were unable to obtain the back transfer rates k'_{7S} from our data.

We note that all our final rates listed in Tables II and III were taken using the cell baked to 650 °C before filling.

Further systematic study of the effects of impurities on sealed cell experiments such as this one are needed and are now underway in our laboratory. This information is crucial to anyone wishing to extract quantitative values for rates from data taken in closed cells.

6. Cs₂(E) state infrared branching

The absolute calibration of Γ_{P7S}, Γ_{P5D}, k_{7S}, and k_{5D} was based on the determination of Γ_E from the zero density intercept of the E state lifetime. In this, however, we assumed that essentially all radiative decay from the E state takes place in the visible E band or near IR cross fluorescence [see Eq. (31)]. A careful search for other possibly significant emissions from the E state was carried out between $\lambda = 0.4$ and $\lambda = 1.8\,\mu m$ without positive results. However, we cannot rule out the possibility of significant branching beyond $\lambda = 1.8\,\mu m$. In fact Amiot et al.[8] have recently observed emission over the entire range 1.0–2.5 μm for Cs_2 excited at 488.0, 496.5, and 514.5 nm. Unfortunately for our purposes, they do not give any indication of relative intensities in these spectral regions. If the branching beyond 1.8 μm is significant, it introduces a systematic error in the results presented here. One type of emission that might have escaped our detection is cascade to a metastable state of the $6P + 6S$ manifold which is collisionally depopulated by excitation transfer to the $b\,^3\Sigma_g^+$, $a\,^3\Pi_u$, or $A\,^1\Sigma_u^+$ state. The main cross fluorescence band between 1.48 and 1.65 μm which we do observe has been attributed to just such a transition $E\,^1\Sigma_u^+ \to {}^1\Pi_g$ except that the wavelengths in this case are within the capabilities of our detectors. It is unlikely that any such infrared emissions are comparable in intensity to the visible and 1.48–1.65 μm bands. However, if such are observed in the future, our results could be modified to take this into account.

7. Polarization and anisotropies in the fluorescence

Systematic errors may be introduced into our results in two different ways if either the atomic or molecular fluorescence is polarized. First, polarization implies anisotropic fluorescence emission which means we were not collecting the same fraction of molecular and atomic fluorescence. Second, our monochromator–photomultiplier system is not equally sensitive to both polarizations. Worse, these effects could be density dependent since collisional processes tend to reduce polarization. We have measured the polarization of the atomic and molecular fluorescence and found that while the atomic fluorescence was unpolarized as expected (since the atomic states were populated by collisions and predissociation), the molecular emission had an average polarization of approximately 30% at both high and low temperatures. This implies that Q as well as P and R lines were present. The lack of temperature dependence to the polarization also indicates that these effects do not influence our measurements of the

density dependencies of I_{7S}/I_E and I_{5D}/I_E. In the absolute fluorescence ratio measurements, we observed at the "magic angle" $\theta = 54.7°$ between the laser polarization and light detection axes, which ensured that we collected the same fraction of molecular and atomic fluorescence. We also placed a linear polarizer in front of the monochromator oriented at 45° with respect to the slits and the projection of the laser polarization onto the plane of the slits which guaranteed that we were equally sensitive to both polarizations.

8. Cascade

Levels lying higher than $7S$ were not significantly populated in this experiment, and therefore cascade effects were neglected in our rate equation analysis. A detailed study of fluorescence from such high lying levels was made (see Ref. 13) and we found that in no case does neglect of cascade lead to more than a 3% error in our results.

9. Power dependencies

A study of I_{7S}, I_{5D}, and I_E vs laser intensity was made to verify that no nonlinear mechanisms of populating the atomic states were important, and that trapping of $7S{\rightarrow}6P$ and $5D{\rightarrow}6P$ fluorescence was negligible. We found that in all cases, the three signals displayed the same laser intensity dependence within experimental uncertainties. Each signal was approximately linear in laser intensity except in the 488.0 nm excitation case where all signals showed saturation behavior at high intensities (see Ref. 13).

10. Stimulated emission and diffusion

The presence of stimulated emission in our lifetime experiment would reduce the E state lifetime and introduce a serious source of uncertainty in our results. This problem was avoided by working at laser intensities that were more than three orders of magnitude smaller than the saturation intensity. Since at the saturation intensity, the stimulated and spontaneous emission rates are roughly equal, we are assured that our lifetime measurements have less than a 0.1% error due to stimulated emission.

Diffusion out of the laser excited column could also reduce the measured lifetime. We have calculated the diffusion time to be $\sim 10^{-5}$ s which is much longer than the E state lifetime. Therefore diffusion can also be safely neglected.

11. Laser and Rayleigh scatter

In the fluorescence measurements of the visible E band, the combination of interference filter and monochromator reduced the contribution of scattered laser light to less than 0.1%. In the absolute measurement of I_{7S}/I_E, the interference filter was not used, but the spike appearing in the spectra as the monochromator passed through the laser wavelength was not included in the band fluorescence. Laser scatter from surfaces and Rayleigh scatter from cesium molecules are more serious problems in the lifetime measurements since there, only the interference filter and not the monochromator was used to observe the molecular fluorescence. The presence of laser or off resonant Rayleigh scatter

(which are both instantaneous and therefore introduce no phase shift) in the fluorescence signal, tends to reduce the apparent lifetime. We estimated the magnitude of this effect by looking at laser scatter in a cold cell. Since this scatter is from oven and cell surfaces, it should be independent of temperature. We found that in the worst case (smallest molecular fluorescence signals at low temperature), scattered laser light contributed less than 4% to the fluorescence. At our highest Cs density we measured the total scattered light signal at the laser wavelength (consisting of laser scatter and Rayleigh scatter), and compared this to the scatter only signal from the cold cell. From this we found that Rayleigh scattering comprised only 14% of the total and therefore its contribution to the fluorescence signal measured in the lifetime experiment was less than 1%.

A more serious problem could arise from Raman scattering within the bandpass of our interference filter. Fluorescence (by which we mean collisionally redistributed light) from a single excited state of an atom or molecule, always yields a phase shift given by $\tan \phi = \omega_m \tau$ (where ω_m is the modulation frequency) independent of laser detuning from the transition frequency, since the emission is redistributed over the full line profile. Rayleigh and Raman scattering introduce phase shifts which depend critically on detuning. Far off resonance, Rayleigh and Raman scattering are in-phase with the excitation source, while at exact resonance the phase shift is given by $\tan \phi = 2\omega_m \tau$. For white light excitation, however, the average phase shift satisfies $\tan \phi = \omega_m \tau$ just as for fluorescence. In our experiment the laser was multimode and broadband, the spectral density of molecular lines was very high, and Doppler and hyperfine effects were present. All of these contributed to produce a situation very similar to the white light excitation case since all possible relative detunings were present. Additionally, at the high densities used in this experiment, we could expect much more collisionally redistributed light than Rayleigh and Raman scattered light. This is corroborated by our high temperature scan of the E band which yields 0.02 as an upper limit for the ratio of Rayleigh scattering to fluorescence.

12. Collisional mixing of dissociation products

Atomic states populated by processes (9) and (10) may undergo excitation transfer to other atomic states before they have a chance to radiate. This should not affect the $7S$ state since it is fairly isolated and has a fast radiative rate. An excitation transfer cross section of several hundred Å^2 would be required to compete significantly with the $7S$ radiative rate which is unreasonable considering $\Delta E > 3200$ cm^{-1}. The $5D$ case is less clear since the radiative rate is an order of magnitude smaller than that for $7S$, but since in this case ΔE is greater than 2700 cm^{-1} which is $\sim 6kT$, we expect no mixing out of $5D$. On the other hand, the two $5D$ fine structure levels might be mixed to some degree since they are only separated by 98 cm^{-1}. If this were so we would only obtain total collisional and predissociation rates into $5D$ without resolution of the contribution to the individual fine structure levels. The two-photon method of Collins et al.[10-12] avoids collisional mixing following population of the atomic state and therefore resolves the individual fine structure level con-

tributions. Our data, however, at all densities studied, yield $I_{5D_{5/2}\to 6S}/I_{5D_{3/2}\to 6S} \sim 2$, whereas the complete mixing ratio $(g_{5/2}/g_{3/2})e^{-\Delta E/kT}$ is 1.1. This value was verified in a cell containing $\sim 1/2$ atmosphere of neon gas where the fluorescence ratio obtained was ~ 1.1. Our data therefore indicate that not much mixing is occurring in our pure cesium cell (the fluorescence ratio is independent of density) and that the $5D_{5/2}$ level is being populated more rapidly by predissociation than the $5D_{3/2}$ level. Thus we present individual rates for $\Gamma_{P5D_{5/2}}$ and $\Gamma_{P5D_{3/2}}$ in Table II which indicate that the ratio of the production rates (as opposed to the steady-state populations) of these two states is approximately statistical. The values of k_{5D} have such high uncertainty that we did not attempt to distinguish them by product fine structure state. These present results are consistent with those of McClintock and Balling[36] who found $I_{5D_{5/2}}/I_{5D_{3/2}} \sim 2.26$ thereby also indicating that $5D_{5/2}$ is populated at a greater rate than $5D_{3/2}$ for 488.0 nm excitation. These results appear at first glance to be inconsistent with those of Collins et al.[10-12] who found that $5D_{3/2}$ is more rapidly populated in a two-photon pulsed experiment. However, it is likely that this apparent discrepancy in the results of the two experiments will be reconciled by considering the role of processes which occur on the different time scales probed by the two experiments. This will be discussed further in Sec. VI.

13. Additional collisional processes

Many other processes, such as molecule–molecule and excited atom–excited atom collisions, etc., could have been included in the rate equations presented in Sec. II. Contributions from such processes were neglected, however, since these collisions are relatively very rare, i.e., $[\text{Cs}_2]/[\text{Cs}] < 10^{-2}$ and $[\text{Cs}(6P)]/[\text{Cs}] < 10^{-4}$ for the temperature range and laser powers of interest. We estimate that neglect of such processes introduces negligible uncertainty in our results.

Uncertainties listed in Tables I–III include systematic uncertainties discussed above as well as purely statistical uncertainties. We believe our estimates of total uncertainties are conservative.

VI. DISCUSSION

We observe a very different radiative lifetime for the levels populated by 465.8 nm light than for those pumped by 488.0 and 514.5 nm excitation. This may imply that we are really observing two or more electronic states as was first suggested by Baumgartner et al.[9] based on their lifetime measurements. In their experiment, however, it was not possible to distinguish between predissociation and radiative decay so that the short lifetime when using shorter wavelengths which pump higher lying vibrational levels, could have been due to passing a predissociation threshold. In the present experiment, we do observe a much larger rate for predissociation to the $7S$ state for the 465.8 nm excitation (this is not surprising since the $7S$ dissociation limit can only be reached from the bottom of the ground state $X \, ^1\Sigma_g^+$ potential well $D_e \sim 3648$ cm^{-1} [37,38] by a photon with $\lambda < 451$ nm). However, we also find that the total radiative rate for 465.8 nm excitation is approximately one third that for the other two

lines. Additionally, we note that the near IR cross fluorescence is absent when using the 465.8 nm pump. All rates obtained using 488.0 and 514.5 nm excitation are in reasonable agreement. We therefore conclude that these two laser lines pump a different electronic state from that pumped by 465.8 nm light.

The lifetime measurements we made with 488.0 nm excitation yield a zero density intercept of $\tau_E = 42.2$ ns which is $\sim 50\%$ larger than the value of 27.0 ± 2 ns obtained by Baumgartner et al.[9] We do not fully understand the causes of this discrepancy. However, we note that most of the possible systematic errors, such as quenching by any impurity gases present and contamination of the fluorescence signal with scattered laser light, tend to result in a measured lifetime that is shorter than the actual lifetime. In particular we do not know if impurities were a problem in the Baumgartner experiment. Our value of 42.2 ns was obtained in a cell baked to 650 °C while a cell baked at only 580 °C resulted in $\tau = 33.9$ ns. In the Baumgartner et al. experiment the cells were only baked to 400 °C before filling. We could attribute the shorter lifetime of the Baumgartner experiment to the presence of impurities in their cells except that they state that in some cases they used sealed cells and in others, cells connected to a vacuum system. Obviously cells connected to a vacuum system would probably contain less impurity gas. We note that the lifetime obtained by Baumgartner et al. for the K₂ $B \, ^1\Pi_u$ state was 9.65 ns while Tango and Zare[39] reported a value of 12.5 ns. On the other hand, the Na₂ $B \, ^1\Pi_u$ state lifetimes reported by Baumgartner et al. are in good agreement with results of McClintock, Demtroder, and Zare[40] who used a molecular level crossing technique.

The present measurements of absolute predissociation rates at fixed wavelengths were meant to complement the measurements of Collins et al.[10-12] of relative photolysis rates to specific fine structure levels of the $5D$ and $6P$ states, as a function of excitation wavelength. We had hoped to put an absolute y-axis scale on the results shown in Fig. 1 of Ref. 12. However the discrepancy between the relative production rates for $5D_{5/2}$ and $5D_{3/2}$ observed in the two experiments casts some doubt on the validity of this approach. As mentioned in Sec. V C12, our results and those of McClintock and Balling[36] imply a statistical ratio for the population rates of $5D_{5/2}$ and $5D_{3/2}$ for the three wavelengths used here, whereas Collins et al. observed preferential population of $5D_{3/2}$. We note, however, that the results of Collins et al. for the relative $6P_{1/2}$, $6P_{3/2}$ population rates for excitation in the C band are consistent with those of Grushevskii et al.[41] and Kraulinya et al.[42] The only major difference between our experiment and that of Collins et al. is in their respective time scales, so we look there for an explanation of the discrepancy in the results. As stated in Sec. II, our definition of predissociation also includes direct dissociation, radiation to directly dissociating states and radiation to predissociating states. All but the last mechanism would make the same relative contribution in the pulsed and cw experiments since a molecule in a directly dissociating state flys apart in approximately one vibrational period ($< 10^{-12}$s) which is fast on the time scale of either experiment. On the other hand, radiation to a predissociating state contributes in the cw ex-

periment but not in the pulsed experiment, since in the latter case the population of the predissociating state does not have time to build up before the second pulse. This type of mechanism, where an intermediate state must build up population before it can contribute to the atomic level population is referred to as a "delayed" source in the language of Ref. 43. "Prompt" sources are those that directly transfer excitation from the molecular E state to the atomic state such as predissociation proper or collisional processes such as Eq. (10). Our cw experiment samples both prompt and delayed processes while the two photon technique has the power to distinguish between the two. In particular, Refs. 10–12 comprise a study of prompt photolytic processes. We note too that in our cw experiment, delayed collisional processes may also exist. For instance, radiation from the E state to a lower bound state which then undergoes excitation transfer with an atom to produce an excited $5D$ atom, would be such a delayed collisional source. Collisional transfer from the E state to a state predissociating to $5D$ is another. All such processes would contribute to our measured values of k_{5D} and k_{7S}. In the $5D$ case at least, these delayed collisional sources are of negligible signficance since k_{5D} itself is very small.

Recent work by Collins and co-workers (Davanloo *et al.*[43]) where the time between pulses was varied over a wide range, indicate that delayed sources of population of the $6P_{1/2}$ and $6P_{3/2}$ states do exist for the laser wavelengths of interest to us. These recent results reconcile an apparent discrepancy between our results and those of Collins' prompt photolysis work[10-12] for the relative production rates for $5D$ and $6P$. It is likely that the apparent discrepancy between our relative $5D_{5/2}$ and $5D_{3/2}$ production rates and those of Refs. 10–12 will also be reconciled by a similar study in which the population rate to each fine-structure level is monitored as a function of time between pulses. As yet, however, no such delayed sources of $5D$ level population have been observed for our excitation wavelengths.[43]

It is important to note the complementary nature of the present work and that of Collins *et al.* Our work provides information on the density dependence which distinguishes collisional terms k_{nL} from spontaneous dissociation terms Γ_{PnL} and also provides absolute determination of these rates at selected wavelengths. The two-photon technique of Collins *et al.* provides time resolution which distinguishes prompt from delayed processes and also yields the relative population rates of the various atomic levels over a broad range of wavelengths. Taken together these two experiments provide (in principle at least) a complete account of the mechanisms for producing excited atoms following absorption of a photon by the cesium molecule.

We note that the excitation transfer from molecule to atom described by Eqs. (10) and (12) is not a true photolysis, but does contribute to the signal observed by Collins *et al.*, since the relative production rates of excited atoms due to spontaneous dissociations and collisional terms is given by Γ_{PnL}/k_{nL} [Cs] independent of the time between their laser pulses. Thus the photolysis cross sections of Collins *et al.* are proportional to $\alpha_\nu (\Gamma_{PnL} + k_{nL} [\text{Cs}])\tau = \alpha_\nu (\Gamma_{PnL} + k_{nL} [\text{Cs}])/(\tau_E^{-1} + k_E [\text{Cs}])$ where α_ν is the absorp-

tion cross section (at these densities, the molecular absorption is simply proportional to α_ν) [Cs] is their cesium density $(2.14 \times 10^{15}$ cm$^{-3})$ and $(\Gamma_{PnL} + k_{nL} [\text{Cs}])\tau$ is the branching ratio for production of atoms in the state nL. In particular our data for 465.8, 488.0, and 514.5 nm excitations indicate that since the k_{5D} are small, the photolysis rates of Collins *et al.* to the $5D$ levels are in fact proportional to predissociation rates, while our large values of k_{6P} imply that at these wavelengths the rates for production of $6P$ atoms [due to delayed sources (see Ref. 43)] are dominated by the collisional mechanism. Due to the presence of delayed sources of population of $5D$ and $6P$ atoms, it is not in general correct to use our results as such to put an absolute y axis scale on the prompt photolysis results of Fig. 1 of Ref. 12. However, the recent two-photon pulsed measurements[43] indicate that delayed sources of $5D_{3/2}$ atoms are not important at 488.0 nm (delayed sources of $5D_{3/2}$ were observed for 514.5 nm excitation, while the 465.8 nm case was not studied in Ref. 43) so that we can obtain a calibration factor C at that wavelength (arbitrary units of Fig. 1 of Ref. 12 $\times C$ = absolute units), which would then read $\alpha_\nu (\Gamma_{PnL} + k_{nL} [\text{Cs}])\tau$, by comparing the total $5D_{3/2}$ population rates in the two experiments. The value obtained at 488.0 nm is $C = 5.8 \times 10^{-18}$ cm^2, where α_ν was measured by us. We believe this value is accurate to within approximately 40%. However, we note that if delayed sources of $5D_{5/2}$ population do not exist for 488.0 nm excitation (this fine structure state was not studied in Ref. 43) then we cannot explain the difference in relative $5D_{3/2}$ and $5D_{5/2}$ population rates observed here and in Ref. 12. Thus the validity of this calibration remains somewhat in doubt until the existence of delayed sources of $5D_{5/2}$ population is demonstrated.

Clearly the infrared branching ratios and depopulation rates of the Cs₂(E) state reported here have implications for the possibility of developing a Cs₂ near IR cross fluorescence laser. In particular it is clear that blue excitation (~465.8 nm) would not be appropriate for this purpose since the IR branching is so small. On the other hand the 488.0 and 514.5 nm excitation cases are more promising since the IR branching is significant and the predissociation and collisional depopulation rates are not too large. Unfortunately little is known about the depopulation mechanisms of the lower state of the IR emission, although Amiot *et al.*[8] have recently identified the state as $^1\Pi_g$ of the $6P + 6S$ manifold with spectroscopic constants which are in good agreement with the recent calculations of Jeung *et al.*[44] We are continuing to study the possibility of a cross fluorescence laser using pulsed excitation which could yield valuable information on the depopulation mechanisms and rates of this $^1\Pi_g$ state and give us a good indication of whether or not a Cs₂ cw cross fluorescence laser is possible.

VII. CONCLUSIONS

We report here absolute rates for predissociation and collisional excitation transfer out of the Cs₂(E) state which result in population of the atomic $7S$, $5D$, and $6P$ levels as well as the total collisional quenching rates for the Cs₂(E) state. These results appear reasonable and indicate that the

predissociation rates are large enough to yield significant populations in the atomic levels.

We also report improved values for the radiative rates and branching ratios of the Cs$_2(E)$ state. These results indicate that the Cs$_2$ "E" absorption band most likely consists of transitions from the ground $X\,{}^1\Sigma_g^+$ state to two or more separate upper electronic states.

Due to the complexity of the rate equations, and the many potential sources of systematic error, our results have fairly large uncertainties. However, we hope they will prove useful in estimating the relative importance of these various processes in laser excited cesium vapors.

Note added in proof: Amiot, Crépin, and Vergés have recently published the results of detailed spectroscopic studies on Ar$^+$ laser-induced fluorescence of the Cs$_2$ molecule [J. Mol. Spectrosc. **107**, 28 (1984)]. These new results verify that we are observing two upper electronic states, and definitely identify them as $^1\Sigma_u^+$ and $^1\Pi_u$.

ACKNOWLEDGMENTS

[1]H. Itoh, H. Uchiki, and M. Matsuoka, Opt. Commun. **18**, 271 (1976).

[2]W. Wellegehausen, S. Shahdin, D. Friede, and H. Welling, Appl. Phys. **13**, 97 (1977).

[3]B. Wellegehausen, IEEE J. Quant. Electron. **15**, 1108 (1979).

[4]J. T. Bahns, K. K. Verma, A. R. Rajaei-Rizi, and W. C. Stwalley, Appl. Phys. Lett. **42**, 336 (1983).

[5]W. Luhs and B. Wellegehausen, Opt. Commun. **46**, 121 (1983).

[6]N. D. Bhaskar, E. Zouboulis, R. Novak, and W. Happer, Chem. Phys. Lett. **63**, 555 (1979).

[7]Z. Wu, M. Ligare, and W. Happer, Phys. Lett. A **89**, 7 (1982).

[8]C. Amiot, C. Crepin, and J. Verges, Chem. Phys. Lett. **98**, 608 (1983).

[9]G. Baumgartner, W. Demtroder, and M. Stock, Z. Phys. **232**, 462 (1970).

[10]C. B. Collins, J. A. Anderson, F. W. Lee, P. A. Vicharelli, D. Popescu, and I. Popescu, Phys. Rev. Lett. **44**, 139 (1980).

[11]C. B. Collins, J. A. Anderson, D. Popescu, and I. Popescu, J. Chem. Phys. **74**, 1053 (1981).

[12]C. B. Collins, F. W. Lee, J. A. Anderson, P. A. Vicharelli, D. Popescu, and I. Popescu, J. Chem. Phys. **74**, 1067 (1981).

[13]Z. Wu, Ph. D. thesis, Columbia University, 1983 (unpublished).

[14]L. Brewer, C. G. James, R. G. Brewer, F. E. Stafford, R. A. Berg, and G. M. Rosenblatt, Rev. Sci. Instrum. **33**, 1450 (1962).

[15]J. K. Link, J. Opt. Soc. Am. **56**, 1195 (1966).

[16]Chr. Bastlein, G. Baumgartner, and B. Brosa, Z. Phys. **218**, 319 (1969).

[17]T. Holstein, Phys. Rev. **72**, 1212 (1947).

[18]T. Holstein, Phys. Rev. **83**, 1159 (1951).

[19]A. N. Nesmeyanov, *Vapor Pressure of the Elements* (Academic, New York, 1963).

[20]E. K. Kraulinya, E. K. Kopeikina, and M. L. Janson, Chem. Phys. Lett. **39**, 565 (1976).

[21]E. K. Kopeikina and M. L. Yanson, Opt. Spectrosc. (USSR) **41**, 217 (1976).

[22]L. K. Lam, T. Fujimoto, A. C. Gallagher, and M. M. Hessel, J. Chem. Phys. **68**, 3553 (1978).

[23]C. G. Carrington, D. N. Stacey, and J. Cooper, J. Phys. B **6**, 417 (1973).

[24]A. C. G. Mitchell and M. W. Zemansky, *Resonance Radiation and Excited Atoms* (Cambridge University, Cambridge, 1934).

[25]E. Milne, J. London Math. Soc. **1**, 40 (1926).

[26]B. P. Kibble, G. Copley, and L. Krause, Phys. Rev. **153**, 9 (1967).

[27]K. Niemax, J. Quant. Spectrosc. Radiat. Transfer **17**, 125 (1977).

[28]B. Warner, Mon. Not. R. Astron. Soc. **139**, 115 (1968).

[29]R. J. Exton, J. Quant. Spectrosc. Radiat. Transfer **16**, 309 (1976).

[30]B. Sayer, R. Wang, J. C. Jeannet, and M. Sassi, J. Phys. B **4**, L20 (1971).

[31]V. K. Prokofev, Z. Phys. **57**, 387 (1929); Zhur. Eksp. Teor. Fiz. **1**, 123 (1931).

[32]S. M. Gidneva and G. A. Kasobov, *Proc. Seventh Int. Conf. on Phenomena in Ionized Gases*, edited by B. Perovic and D. Tosic (Gradevinska Knjiga, Belgrade, 1965), Vol. II, p. 581.

[33]I. V. Hertel and K. J. Ross, J. Phys. B **2**, 484 (1969).

[34]J. Huennekens and A. Gallagher, Phys. Rev. A **27**, 1851 (1983).

[35]T. P. Whaley, in *Comprehensive Inorganic Chemistry*, edited by J. C. Bailar, H. J. Emeléus, Ronald Nyholm, and A. F. Trotman-Dickenson (Pergamon, Oxford, 1973), Vol. I, p. 369–531.

[36]M. McClintock and L. C. Balling, J. Quant. Spectrosc. Rad. Transfer **9**, 1209 (1969).

[37]M. Raab, G. Honing, W. Demtroder, and C. Vidal, J. Chem. Phys. **76**, 4370 (1982).

[38]M. Raab, H. Weickenheimer, and W. Demtroder, Chem. Phys. Lett. **88**, 377 (1982).

[39]B. Tango and R. N. Zare, results quoted in Ref. 9.

[40]M. McClintock, W. Demtroder, and R. N. Zare, J. Chem. Phys. **51**, 5509 (1969).

[41]V. B. Grushevskii, S. M. Papernov, and M. L. Yanson, Opt. Spectrosc. **44**, 475 (1978).

[42]E. K. Kraulinya, S. M. Papernov, and M. L. Janson, Chem. Phys. Lett. **63**, 531 (1979).

[43]F. Davanloo, C. B. Collins, A. S. Inamdar, N. Y. Mehendale, and A. S. Naqvi (to be published).

[44]G. H. Jeung, F. Spiegelmann, J. P. Daudey, and J. P. Malrieu, J. Phys. B **16**, 2659 (1983).